INSTITUTE OF PHYSICS PUBLISHING NANOTECHNOLOGY
Nanotechnology **17** (2006) 1272–1277 doi:10.1088/0957-4484/17/5/019

Control of topography, stress and diffusion at molecule–metal interfaces

Nikolai B Zhitenev[1,5], Weirong Jiang[1,2], Artur Erbe[3], Zhenan Bao[4], Eric Garfunkel[2], Donald M Tennant[1] and Raymond A Cirelli[1]

[1] Bell Labs., Lucent Technologies, Murray Hill, NJ 07974, USA
[2] Department of Chemistry, Rutgers University, Piscataway, NJ 08854, USA
[3] Fachbereich Physik, Universität Konstanz, 78464 Konstanz, Germany
[4] Department of Chemical Engineering, Stanford University, Stanford, CA 94305, USA

E-mail: zhiten@lucent.com

Received 14 October 2005
Published 7 February 2006
Online at stacks.iop.org/Nano/17/1272

Abstract
The transport properties of metal–molecule–metal junctions containing a monolayer of conjugated and saturated molecules with characteristic dimensions in the range 30–300 nm are correlated with microscopic topography, stress and chemical bonding at the metal–molecule interfaces. Our statistically significant dataset allows us to conclude that the conductivity of organic molecules ∼1.5 nm long is at least four orders of magnitude lower than is commonly believed.

(Some figures in this article are in colour only in the electronic version)

1. Introduction

Reliable and scalable integration of organic molecules within nanoscale electronic devices has the potential to dramatically expand available device functionality. Similarly to other device platforms such as Si-based technology, the electronic properties of devices that are just a few atomic layers thick are determined not solely by the properties of the host material but are equally dependent on dopants, defects and electronic states at the interfaces. The incorporation of molecules in small devices calls for the simultaneous solutions of many interrelated material, electronic and chemical issues. In this paper, we focus on devices built of self-assembled molecular layers (SAMs) enclosed between two metal electrodes [1–3]. Typically, organic molecules do not have electronic states at the energy close to the Fermi energy of common metals. Electrons travel between metal electrodes by tunnelling through the molecules in the gap between the highest occupied (HOMO) and lowest unoccupied (LUMO) molecular orbitals. Tunnelling transmission is governed by the energy difference between the Fermi level of the contacts and the closest molecular orbital and by the spatial extent of the molecular orbital. Because of the exponential sensitivity of tunnelling transmission to energy and distance, the conductance of real devices can be much larger or much smaller than that from molecular tunnelling.

A single state in a molecular layer with defect energy close to the Fermi energy can dramatically increase the transmission. The most common origin of defects in molecular devices is the penetration of metal contacts into the molecular layer. During and after fabrication, metal filaments can form, either completely shorting the source and the drain electrodes and limiting the yield of useful devices [4, 5], or strongly increasing the device conductance [6]. Metal particles can penetrate into the molecular layers [7]. In the process of the metal contact film growth and crystallization the electrode can protrude into the layer, thus deforming molecules and affecting the conductance [8]. On the other hand, distorted chemical bonds at the interface between the metal and the molecule can decrease the tunnelling transmission. Metal films commonly used for electrodes, for example, Au, Ag, Ti, Pt, grow and interact very differently on top of molecular layers [9–12]. Currently, every experiment is unique in that the atomic placement of the relevant device constituents cannot be determined accurately.

The main goal of the paper is to study the phenomena affecting the conductance of molecular devices by systematically varying the growth conditions at the metal–molecule interface. Specifically, first we optimize the surface topography of the metal electrode used for the assembly of the molecular layer reducing the density of structural defects in the SAM.

[5] Author to whom any correspondence should be addressed.

This dramatically reduces the diffusion of the top metal contact through the molecular layer, increasing the device yield to >90%. Then, we experiment with the chemical bonding and surface topography at the top metal–molecule interface.

2. Experimental details

The general approach for molecular device fabrication is to perform the most critical patterning of nanometre features without molecules, assemble the molecules, and to complete the structure with a relatively non-invasive processing step. We use small shadow masks defined within a stack of $SiO_2/SiN_x/SiO_2$ layers grown on degenerately doped Si substrates to obtain features below the lithographic limit [5, 13–16]. A layer of SiO_2 (200 nm) is grown on Si to isolate the substrate from the devices. Oxide is then removed in 5 μm by 5 μm central windows. Next, Si_3N_4 (400 nm) and SiO_2 (150 nm) mask forming layers are deposited. The desired pattern is defined by photolithography and etching of the top SiO_2 layer. Si_3N_4 is selectively etched undercutting the top SiO_2. Finally, high quality 10 nm SiO_2 is regrown on the exposed Si surface allowing the use of the doped substrate as gate electrode. The fabrication of metal–SAM–metal junctions using the masks is illustrated in figure 1. First, the bottom electrodes are defined by evaporation. In the current study, the bottom electrode is Ti/Au (5 A/300 A). The electrodes are separated by a bridge with a width in the range 100–300 nm. Next, a SAM is deposited from solution in the usual manner. Two types of molecule, representing opposite ends of expected electronic functionality, are used in this study. Terthiophenedithiol (T3), synthesized using previously described methods [17], is a conjugated molecule with thiol groups responsible for chemical attachment to metal electrodes. Decanedithiol (C10) is a fully saturated molecule with a length of 1.5 nm similar to the T3 length. The substrates with bottom Au electrodes were soaked in a tetrahydrofuran (THF) solution of the thiols (about 0.01 mM) at room temperature for 24 h, then rinsed with THF, toluene and isopropanol. Both molecules form SAMs with thiol terminations exposed at the top interfaces as proven by nanotransfer experiments [18]. Finally, a top electrode is evaporated through the same mask from a different angle. The size of the junction is controlled by the size of the bridge and the angle of the second evaporation. SEM images of representative junctions are shown in figure 1(c). A single chip contains 84 separate devices, allowing us to perform a statistical analysis on nominally equivalent junctions and to vary the junction sizes. The electrical characterization does not require the removal of the mask stack or metal accumulated on top surface of the mask, thus minimizing this potential source of damage or contamination.

3. Results

In the first experiments, we assembled both molecules on an as-deposited Au electrode. The top electrode was an 8 nm Au or Ag film. The resistance of all junctions appeared to be indistinguishable from the lead's resistance, which is in the range 300 Ω–1 kΩ for devices with different lead geometries. We conclude that the evaporated metal penetrates through the

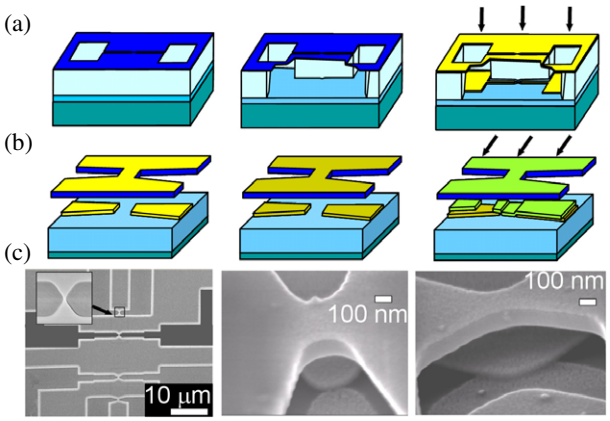

Figure 1. Fabrication of templates and molecular junctions. (a) The stencil mask is defined within an insulating stack of SiO_2/Si_3N_4 layers grown on Si substrate. A layer of SiO_2 (10 nm in 5 μm by 5 μm central windows, 200 nm elsewhere on the wafer) is grown on Si (bottom layer) to isolate the substrate from the devices followed by Si_3N_4 (∼400 nm) and SiO_2 (∼150 nm, top layer) mask forming layers. The desired pattern is defined by photolithography and etching of the top SiO_2 layer. Si_3N_4 is selectively etched undercutting the top SiO_2. The mask is used to define the pattern of evaporated metal electrodes. The metal accumulated on the top surface of the mask is electrically isolated from the evaporated electrodes. (b) Fabrication of a molecular junction using the template. The bottom electrodes are defined on the substrate by evaporation. A molecular layer is deposited from solution. Evaporation of the second electrode from an angle completes the junction. (c) SEM images of the template (one out of four shown samples is shaded) and examples of small and large junctions.

SAMs shorting the devices. These results are consistent with our earlier observation of a low yield of non-shorted multi-grain junctions formed with different nanotemplates [19]. The evaporated top metal easily diffuses near defects in molecular packing induced by multiple grain boundaries of the bottom electrode.

In the next set, we annealed (250 °C, 5 min) the chips after deposition of the bottom Au contact. The annealing modifies the grain structure of polycrystalline Au film, making the grains smoother and the grain size larger. The distribution of device resistances measured at room temperature is shown in figure 2(a). Although the variation is very broad, the yield of non-shorted devices is above ∼96% for T3 and ∼92% for C10 SAMs; this is much higher than in previous experiments by others (0.5%–5%) with similar electrode arrangements [4, 5, 15]. Surprisingly, the apparent median resistance for T3 devices is higher than for C10 devices, contrary to all expectations. This clearly shows that the conductance of real junctions is not directly determined by the electronic structures of the molecules. No scaling of the resistance with the junction area is observed.

To study bond formation at the top interface, we used overlayers of metals with different chemical reactivities. Au, Ag or Ti (7 nm) were studied (figure 2). Silver is more reactive than Au, and titanium is known to strongly react not only with thiol groups at the top interface but also with carbon atoms [12]. The electrical properties of T3–Ag junctions are generally similar to those of T3–Au junctions. A significant percentage of the C10–Ag junctions were shorted. The

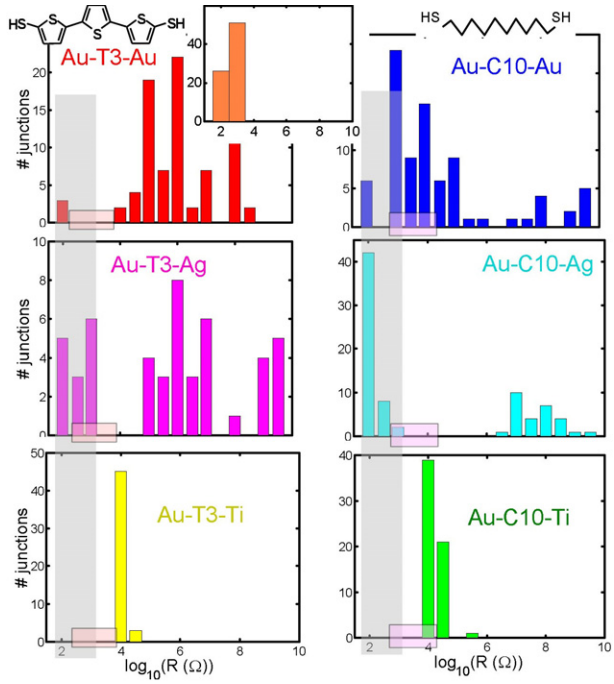

Figure 2. Distribution of junction resistances measured at room temperature. The resistance range corresponding to the lead's resistance is grey coloured (shorted junctions). Short bars show expected ranges of resistances assuming (i) that all molecules inside junctions are bonded to both electrodes and (ii) tunnelling conductance of 10^{-6}–10^{-8} Ω^{-1}/T3 and 10^{-8}–10^{-9} Ω^{-1}/C10. The inset in the top row shows results for junctions fabricated on an as-deposited Au electrode.

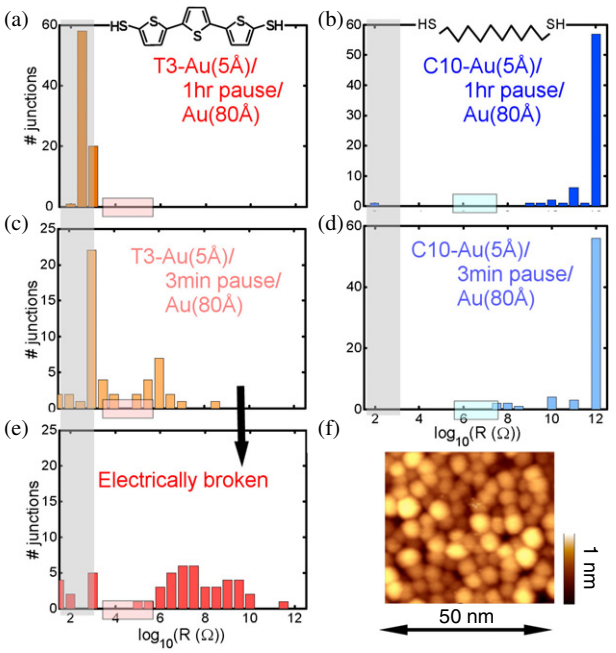

Figure 3. Distribution of junction resistances with the clusters created at the top metal–molecule interface. The top metal contact is formed by depositing 0.5 nm of Au film first, letting the film relax for time τ_{rel}, and depositing another 8 nm of Au: (a) $\tau_{rel} = 1$ h, T3 SAM; (b) $\tau_{rel} = 1$ h, C10 SAM; (c) $\tau_{rel} = 3$ min, T3; (d) $\tau_{rel} = 3$ min, C10. (e) Distribution of junction resistance from (c) after the soft electrical breakdown. Short bars show the expected range of resistances assuming (i) that only one molecule per cluster forms good bonds at both ends and (ii) tunnelling conductance of 10^{-6}–10^{-8} Ω^{-1}/T3 and 10^{-8}–10^{-9} Ω^{-1}/C10; (f) STM image of clusters formed on top of the T3 SAM.

conductance of the junctions with Ti overlayers is consistently higher. The overall histograms are very similar for both T3 and C10 SAMs.

The microscopic topography at the top SAM–metal interface is generally unknown. In an attempt to control the topography, we intentionally created clusters at the top interface. First, 0.3–0.5 nm of Au was evaporated on top of the SAM, simultaneously on the chips and on reference SAMs assembled on an atomically flat Au substrate. The evaporation chamber was vented, and the reference sample was used to examine the topography of the overlayer by STM. Clusters with average diameter ∼6 nm are clearly seen (figure 3(f)). The junction fabrication was completed by evaporating an 8 nm thick film of Au. The electrical properties of the junctions change dramatically in comparison with the uninterrupted Au evaporation, as shown in figures 3(a) and (b). All T3 junctions are shorted while all C10 junctions are highly resistive (for convenience, we lump all $R > 10^{12}$ Ω in a single bin).

In the next experiment, after deposition of 0.5 nm of Au, the evaporation was interrupted for 3 min followed by continuous evaporation of 8 nm of Au (figures 3(c) and (d)). The results clearly fall between the continuous Au evaporation shown in figure 2 and the previous experiment. Half of the T3 junctions are not shorted, and the C10 junctions are less resistive on average. The shorted T3 junctions can be electrically driven into a more resistive state. A voltage pulse with ∼30–50 mV amplitude and rise time below 1 μs usually triggers modification of the shorted junctions. We note that applying a dc voltage up to 1 V does not change the junction conductance. The distribution of resistances of junctions after the breakdown is shown in figure 3(e).

The junction resistance measured at room temperature only partly characterizes the transport properties. We studied the conductance of the junctions as a function of source–drain voltage and temperature. The specific details of the current–voltage (I–V) curves vary significantly as can be expected from the broad distribution of conductance values. Some representative results are illustrated in figure 4.

The transport characteristics of all T3–Ti and C10–Ti junctions are quite similar (figure 4(a)). The conductance falls only by 5–15% as the temperature changes from 300 to 4.2 K. The low-temperature dI/dV curves are rather smooth, with a small dip near zero. The lower conductance, the zero-bias dip and the smooth dI/dV variation clearly differentiate these junctions from shorted ones. Weak temperature dependence and zero-bias anomaly are the usual signatures of tunnelling conductance. Most of the non-shorted C10–Ag and all C10–Au_{clust} junctions also display insignificant temperature dependence but the tunnelling conductance in this case is lower by orders of magnitude in comparison with Ti overlayer junctions. A small percentage of other types of junctions also display a weak temperature dependence of the conductance.

The transport properties of the majority of other junctions with Au and Ag overlayers are more complicated. The I–V curves are usually linear at room temperature.

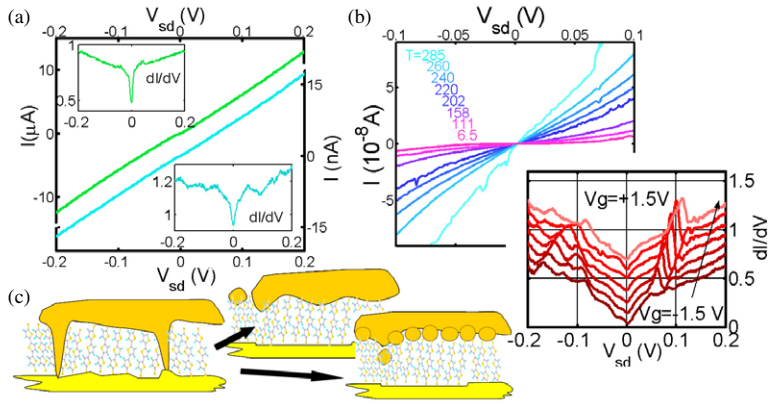

Figure 4. Examples of characteristic transport behaviour. (a) I–V curves measured on C10–Ti (top) and C10–Ag (bottom) junctions. The current scales are different. $T = 8$ K. Insets: corresponding differential conductance $\mathrm{d}I/\mathrm{d}V$ as a function of V_{sd}; (b) I–V curves measured at different temperatures on a C10–Au junction. Inset: set of $\mathrm{d}I/\mathrm{d}V$ curves measured on a T3–Au junction at different gate voltages. $T = 8$ K. (c) Schemes of metal assembly and penetration into the molecular layer illustrating the material modifications and interface topography studied in this paper. Junctions assembled on rough Au surfaces are usually shorted because of easy metal diffusion along structural defects of the SAM. The yield of non-shorted junctions is high if the bottom Au electrode is annealed before the SAM deposition. Metal electrodes can protrude into the SAM volume and/or deform molecules. Relaxation of the thin metal underlayer reduces the stress at the interface.

The conductance measured at zero source–drain bias falls noticeably with decreasing temperature (figure 4(b)). The low-temperature I–V curves display a non-linear region with characteristic voltage scale $V_{\mathrm{sd}} \sim$ 25–200 mV. This general behaviour is typical for T3–Au, C10–Au, T3–Ag, and T3–$\mathrm{Au_{clust}}$ junctions. Similar behaviour has been observed in our previous study of multi-grain junctions fabricated on the tips [19] and it has been analysed in our previous publications [19, 20]. Two separate conductance mechanisms contribute to the overall electrical transport. The temperature-dependent part of the conductance can be identified as hopping transport, characterized by a small energy scale in the range ∼10–150 meV. The residual conductance observed at low temperature is a combination of direct tunnelling between contacts, sequential tunnelling through low-energy defect states, and hopping. The relative contributions of hopping and tunnelling to the overall conductance vary broadly from sample to sample.

Finer differences between transport behaviour in T3 and C10 SAMs can be seen in the low-temperature $\mathrm{d}I/\mathrm{d}V$ curves. The conductance peaks shown in figure 4(b) are observed in most of the T3–Au, T3–Ag and T3–$\mathrm{Au_{clust}}$ junctions. The positions of the peaks on the $\mathrm{d}I/\mathrm{d}V(V_{\mathrm{sd}})$ curves can be shifted by gate voltage in the case of T3–Au and T3–Ag junctions. Such behaviour is reminiscent of single-electron charging of isolated islands. In T3–$\mathrm{Au_{clust}}$ junctions, the peaks are stronger relative to the smoother background while the peak positions are usually insensitive to the gate voltage. No similar conductance peaks were observed in the majority of C10–Au samples.

4. Discussion

First, we comment on overall conductance values through the SAM comparing with previously published results. The commonly accepted [21] tunnelling conductance per conjugated molecule of comparable length [22, 23] is 10^{-6}–10^{-8} Ω^{-1} and the conductance per alkane molecule [24] is 10^{-8}–10^{-9} Ω^{-1}. A median junction ∼100 nm by 100 nm contains $\sim 5 \times 10^4$ molecules. If one assumes that every molecule is well-bonded on both sides, the median resistance of junctions is 20 Ω–2 kΩ and 2–20 kΩ for, respectively, T3 and C10 junctions as illustrated in figure 2 by light coloured rectangles. In most cases, the median experimental resistances are much larger than the estimations based on the literature data. Certainly, the common assumption that all molecules are connected to both contacts can be unrealistic but the experiment with cluster formation at the top interface allows us to reliably estimate the minimal number of connected molecules. If we conservatively assume having just a single bond per metal cluster of the top contact, a representative junction contains ∼300 well-bonded molecules. The corresponding resistance estimates are 3–300 kΩ for T3 junctions, and 300 kΩ–3 MΩ for C10 junctions (shown in figure 3). Clearly, the results show that the tunnelling conductance of molecules is lower by 4–6 orders of magnitude for both conjugated and saturated molecules, in strong contrast to the majority of previous calculations and experiments [21].

In fact, in the vast majority of devices we cannot single out the conductance associated with tunnelling through the molecular orbitals. High values of tunnelling conductance measured in the junctions with Ti overlayers are unlikely to be related to the electronic structures of the original molecules since no difference between conjugated and saturated molecules is seen in the experiment. Evaporated Ti reacts strongly with organics [12] attacking the SAM and forming Ti carbides and oxycarbides. The tunnelling conductance measured in all other junctions is likely to be determined by the microscopic configuration of metal electrodes that have partly penetrated the SAM, and/or a small number of defect states rather than by molecular states.

The essential material transformations defining the electronic properties of molecular junctions are schematically

illustrated in figure 4(c). Structural defects in SAMs assembled on as-deposited Au allow for easy diffusion of the top metal electrode through the layer. The SAM structure is significantly improved by annealing Au films before the deposition of molecules. The high yield of non-shorted devices achieved by evaporation of Au on top of SAMs suggests that practically all incident Au atoms are stopped at the top interface. The overall electrical properties of junctions formed with T3 and C10 SAMs are rather similar. We believe that during its growth and crystallization the Au overlayer penetrates deep into the SAM, exerting substantial pressure and deforming the molecules. The microscopic details of the electrode topography are almost independent of the molecule type in this particular case. Diffusion and growth of Ag overlayers differ depending on the SAM type. Silver penetrates alkane SAMs more easily. Finally, evaporated titanium can react strongly with SAMs, modifying the electronic structure with little discrimination between conjugated and saturated molecules.

Relaxation of the thin Au overlayer accumulated at the top molecular interface and cluster formation result in two new phenomena. First, comparing properties of the junctions formed on C10 SAMs, we suggest that this relaxation significantly reduces the stress at the interface and the penetration of the top metal contact into the SAM volume. The C10 junctions with a relaxed top interface are so resistive that their conductance cannot be reliably differentiated from a possible leakage through the substrate. Very different behaviour is seen on conjugated SAMs. Effectively, the clusters diffuse through the SAM more easily than separate Au atoms impinging the SAM during the evaporation. The cluster diffusion has to proceed along with a redistribution of molecules in the SAM. Apparently, the configuration with the clusters partly or fully submerged into conjugated SAM lowers the total energy of the system. The clusters that form at the edge of a continuous Au top electrode and partly penetrate into the SAM can account for the systematic observation of conductance resonances sensitive to the gate voltage in T3 junctions.

Residual impurities, clusters, other low-energy defects and interface topography leading to different conductance mechanisms and a broad distribution of junction resistances enormously complicate a reliable determination of the tunnelling conductance through the molecular levels. While a significant disagreement with the literature data can be easily demonstrated based on the full dataset, to estimate the molecular conductance we select the more resistive junctions with I–V curves displaying negligible contribution from the low-energy transport channels. The estimates give $R_{T3} > 10^{11}$ Ω and $R_{C10} > 10^{14}$–10^{15} Ω for T3 and C10 respectively. A simple approximation of tunnelling under a rectangular barrier is often useful to relate the values of tunnelling resistances with the energy structure. In such a model, $R = R_0 \exp(\beta l)$, where R_0 is of the order of the quantum resistance, l is the length of the barrier, $\beta = 2(2m^*E)^{1/2}/\hbar$ is the tunnelling decay parameter, E is the barrier height and m^* is the effective mass. Based on the estimates of resistances, $\beta_{C10} \sim 1.5$ and $\beta_{T3} \sim 1.1$, and, assuming $E_{C10} \sim 5$ eV and $E_{T3} = 1.4$ eV (∼1/2 of bandgap), $m^*_{C10} \sim 0.4\ m_0$ and $m^*_{T3} \sim 0.8\ m_0$, where m_0 is the free electron mass. We note that in other well-studied tunnel barriers such as AlO_x and SiO_2 the effective mass is usually close to $0.5\ m_0$ [25, 26]. Calculations of molecular tunnelling if reduced to the simple single barrier approximation typically predict much smaller m^* values such as $m^* \sim 0.2\ m_0$ for alkanes and $m^* \sim$ (0.06–0.25) m_0 for different conjugated molecules [21, 24, 27].

The results clearly expose a variety of material transformations and self-organization processes occurring during the integration of organic and inorganic components in nanoscale devices. This is the first experimental research that systematically correlates the electrical properties of SAM-based molecular devices with the microscopic details of the metal–molecule interface. We have demonstrated that the generation of defects can be dramatically reduced for certain combinations of metals and molecules by changing the surface topography and growth conditions at the interface.

Acknowledgments

We would like to acknowledge useful discussions with E Chandross and D Hamann.

References

[1] Collier C P, Mattersteig G, Wong E W, Luo Y, Beverly K, Sampaio J, Raymo F M, Stoddart J F and Heath J R A 2000 [2]Catenane-based solid state electronically reconfigurable switch *Science* **289** 1172

[2] Chen J, Reed M A, Rawlett A M and Tour J M 1999 Large on-off ratios and negative differential resistance in a molecular electronic device *Science* **286** 1550

[3] Chen Y, Jung G Y, Ohlberg D A A, Li X M, Stewart D R, Jeppesen J O, Nielsen K A, Stoddart J F and Williams R S 2003 Nanoscale molecular-switch crossbar circuits *Nanotechnology* **14** 462

[4] Lee T, Wang W, Zhang J J, Su J, Klemic J F and Reed M A 2005 Cross-platform characterization of electron tunnelling in molecular self-assembled monolayers *Curr. Appl. Phys.* **5** 213

[5] Austin M D and Chou S Y 2003 Fabrication of a molecular self-assembled monolayer diode using nanoimprint lithography *Nano Lett.* **3** 1687

[6] Lau C N, Stewart D R, Williams R S and Bockrath M 2004 Direct observation of nanoscale switching centers in metal/molecule/metal structures *Nano Lett.* **4** 569

[7] Philipp G, Muller-Schwanneke C, Burghard M, Roth S and von Klitzing K 1999 Gold cluster formation at the interface of a gold/Langmuir–Blodgett film/gold microsandwich resulting in Coulomb charging phenomena *J. Appl. Phys.* **85** 3374

[8] Son K-A, Kim H I and Houston J E 2001 Role of stress on charge transfer through self-assembled alkanethiol monolayers on Au *Phys. Rev. Lett.* **83** 5357

[9] Ohgi T, Sheng H-Y, Dong Z-C, Nejoh H and Fujita D 2001 Charging effects in gold nanoclusters grown on octanedithiol layers *Appl. Phys. Lett.* **79** 2453

[10] Ohgi T, Fujita D, Deng W, Dong Z C and Nejoh H 2001 Scanning tunnelling microscopy and X-ray photoelectron spectroscopy of silver deposited octanethiol self-assembled monolayers *Surf. Sci.* **493** 453

[11] Boer B d, Frank M M, Chabal Y J, Jiang W, Garfunkel E and Bao Z 2004 Metallic contact formation for molecular electronics: interactions between vapor-deposited metals and self-assembled monolayers of conjugated mono- and dithiols *Langmuir* **20** 1539

[12] Walker A V, Tighe T B, Stapleton J, Haynie B C, Upilli S, Allara D L and Winograd N 2004 Interaction of vapor-deposited Ti and Au with molecular wires *Appl. Phys. Lett.* **84** 4008

[13] Fulton T A and Dolan G J 1987 Observation of single-electron charging effects in small tunnel junctions *Phys. Rev. Lett.* **59** 109
[14] Kagan C R, Afzali A, Martel R, Gignac L M, Solomon P M, Schrott A G and Ek B 2003 Evaluations and considerations for self-assembled monolayer field-effect transistors *Nano Lett.* **3** 119
[15] Lee J O, Lientschnig G, Wiertz F, Struijk M, Janssen R A J, Egberink R, Reinhoudt D N, Hadley P and Dekker C 2003 Absence of strong gate effects in electrical measurements on phenylene-based conjugated molecules *Nano Lett.* **3** 113
[16] Zhitenev N B, Meng H and Bao Z 2002 Conductance of small molecular junctions *Phys. Rev. Lett.* **88** 226801
[17] Boer B d, Meng H, Perepichka D F, Zheng J, Frank M M, Chabal Y J and Bao Z 2003 Synthesis and characterization of conjugated mono- and dithiol oligomers and characterization of their self-assembled monolayers *Langmuir* **19** 4272
[18] Jiang W R, Zhitenev N B, Bao Z, Meng H, Abusch-Magder D, Tennant D and Garfunkel E 2005 Structure and bonding issues at the interface between gold and self-assembled conjugated dithiol monolayers *Langmiur* **21** 8751
[19] Zhitenev N B, Erbe A and Bao Z 2004 Single- and multigrain nanojunctions with a self-assembled monolayer of conjugated molecules *Phys. Rev. Lett.* **92** 186805
[20] Zhitenev N B, Erbe A, Bao Z, Jiang W and Garfunkel E 2005 Molecular nano-junctions formed with different metallic electrodes *Nanotechnology* **16** 495
[21] Salomon A, Cahen D, Lindsay S, Tomfohr J, Engelkes V B and Frisbie C D 2003 Comparison of electronic transport measurements on organic molecules *Adv. Mater.* **15** 1881
[22] Kergueris C, Bourgoin J P, Palacin S, Esteve D, Urbina C, Magoga M and Joachim C 1999 Electron transport through a metal–molecule–metal junction *Phys. Rev.* B **59** 12505
[23] Heurich J, Cuevas J C, Wenzel W and Schon G 2002 Electrical transport through single-molecule junctions: from molecular orbitals to conduction channels *Phys. Rev. Lett.* **88** 256803
[24] Tomfohr J K and Sankey O F 2002 Complex band structure, decay lengths, and Fermi level alignment in simple molecular electronic systems *Phys. Rev.* B **65** 245105
[25] Cimpoiasu E, Tolpygo S K, Liu X, Simonian N, Lukens J E, Likharev K K, Klie R F and Zhu Y 2004 Aluminum oxide layers as possible components for layered tunnel barriers *J. Appl. Phys.* **96** 1088
[26] Stadele M, Sacconi F, Carlo A and Lugli P 2003 Enhancement of the effective tunnel mass in ultrathin silicon dioxide layers *J. Appl. Phys.* **93** 2681
[27] Joachim C and Magoga M 2002 The effective mass of an electron when tunnelling through a molecular wire *Chem. Phys.* **281** 347